

Direct Experimental Observation of Fracton Mode Patterns in One-Dimensional Cantor Composites

F. Craciun,^(a) A. Bettucci, E. Molinari, A. Petri, and A. Alippi^(a)

Consiglio Nazionale delle Ricerche (CNR), Istituto di Acustica "O. M. Corbino," Via Cassia 1216, I-00189 Roma, Italy

(Received 8 October 1991)

By measuring fracton mode displacements in artificial piezoelectric composites with hierarchical structure, we find direct evidence of their localized and self-similar character. Clear indications of the existence of multiple fracton and phonon regimes are also presented.

PACS numbers: 63.20.Pw, 43.20.+g, 62.65.+k, 63.50.+x

The transition between extended-vibration (*phonon*) regimes and a localized-mode (*fracton*) regime in fractal structures has been the subject of several theoretical investigations [1] since the first studies on fractons [2]. Two crossover wavelengths have been identified, λ_1 and λ_2 , such that modes with wavelength λ larger than a correlation length ξ ($\lambda > \lambda_1 = \xi$) are extended phonons with dispersion $\omega \sim 1/\lambda$, whereas vibrations with wavelength shorter than the smallest-particle size a ($\lambda < \lambda_2 = a$) are essentially the modes of the individual constituent particles. In the intermediate frequency range ($\lambda_2 < \lambda < \lambda_1$) the new fracton excitations are expected, with dispersion relation $\omega \sim \lambda^{-D/d_s}$. Here D and d_s are the fractal and spectral dimensions, respectively, the latter being the exponent characterizing the smooth behavior of the density of states (DOS) in the fracton regime.

On the experimental side [3], evidence for the different mode behavior has been obtained especially from the extensive work in silica aerogels by Courtens, Vacher, and Stoll, who measured the DOS by several complementary techniques [3(e)]. However, the pattern of vibration modes could not be directly probed so far, so that the different localization of modes is usually deduced from the scaling behavior of the DOS.

In the present work we have adopted a different approach. By constructing suitable artificial one-dimensional fractal (Cantor) structures with piezoelectric ceramic and resin constituents we are able to excite vibrations over a wide frequency range ($10 \text{ kHz} < \omega < 5 \text{ MHz}$) and to measure not only the frequency spectrum, but also the surface amplitude of the individual vibration modes. Our experimental mode patterns and frequency spectrum are successfully compared with the predictions of a scalar model, previously tested on several periodic samples [4].

The main results are the direct evidence of the localized character and self-similar nature of fracton displacement patterns, and the existence of further fracton regimes at wavelengths shorter than the "particle size" a , corresponding to localized modes in the gaps between successive harmonic bands of extended modes.

Our samples are composite plates formed by alternating elements of piezoelectric ceramic and epoxy resin, following a triadic Cantor sequence [5] up to the fourth generation (a total of 31 elements). The geometry of the

sample is presented in Fig. 1. Cladding ceramic elements are added at the ends of the sample. The two constituent materials are selected to have a very large difference in acoustic impedance $z = \rho v$, ρ and v being the mass density and relevant sound velocity. As we will see below, this is important to allow the existence of large and well-defined fracton frequency ranges in spite of the relatively small number of generations. The width l of the smallest layers of ceramic and epoxy was chosen such that the acoustic path is the same in both elements (for ceramic $l = 0.8 \text{ mm}$ and for resin $l = 0.453 \text{ mm}$). This gives a crucial simplification in the frequency spectrum (see below). The thickness of the plate (0.3 mm) was designed in such a way that the lowest Lamb mode (S_0) [6] propagates as an effective scalar mode to a very good approximation, as demonstrated in Ref. [4] on periodic structures.

In order to probe the vibration spectra, highly reflecting Al electrodes are deposited on both surfaces of the plates; the admittance function is then measured in a bridge meter. Typical admittance curves (Fig. 2) present a series of maxima when resonant modes of the plate are electrically excited. The increasing background is due to the tail of the large "thickness resonance" (mode S_1) at $\omega/2\pi \approx 5 \text{ MHz}$. Only modes symmetrical with respect to the free ends of the plate are excited [4]. The vibration amplitude is measured at each of these frequencies by an interferometric optical technique whereby a He-Ne laser beam is split in a Mach-Zehnder interferometer; a part of the beam, perpendicularly incident on the sample surface, is phase modulated by the sample vibration and suitably recombined with the unperturbed beam. This heterodyne technique allows local detection of the normal component of the surface displacement (magnitude and phase) down to 10^{-3} \AA [4(c)]. Examples of vibration amplitude profiles obtained by scanning the sample across the different elements are shown in Fig. 3 and will be dis-

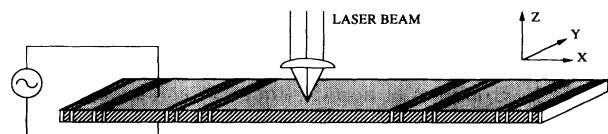


FIG. 1. Sketch of the experimental setup; an electric field applied on the electrodes excites Lamb waves which are propagating along the plate. The normal displacement component is measured by an interferometric laser probe.

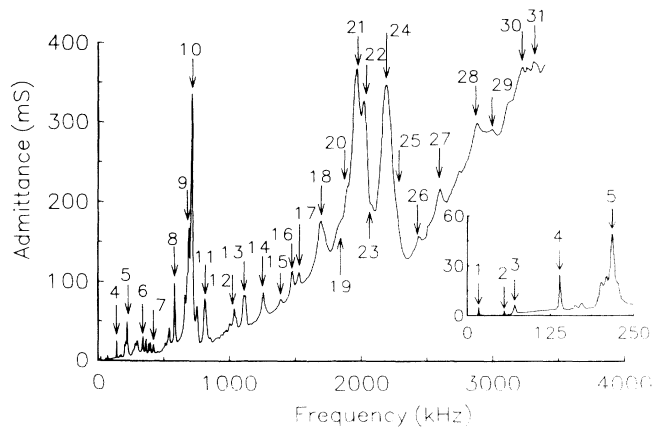


FIG. 2. Raw experimental admittance curve vs frequency for a sample with four generations. The lowest part of the spectrum is enlarged in the inset. The numbered arrows indicate the peaks which have been identified on the basis of their measured displacements and are reported in Fig. 4.

cussed below.

A simple one-dimensional model is used to calculate the frequency spectrum and the normal displacement amplitude of the plate surface. This is possible because we are interested in the frequency range where only the lowest (symmetric) plate mode, the S_0 Lamb mode, is excited. Moreover, as this mode is prevalingly longitudinal [6], the effective velocities may be taken as constants in each material. From the acoustic impedances of both materials, z_1 and z_2 , the reflection coefficient at the interface between medium 1 and medium 2 is simply obtained as $r_{12} = (z_1 - z_2) / (z_1 + z_2)$; at the opposite interface, $r_{21} = -r_{12}$. The transmission of the whole structure is then iteratively obtained by a transfer matrix method, at any frequency. The resulting transmission function is characterized by a series of peaks corresponding to the

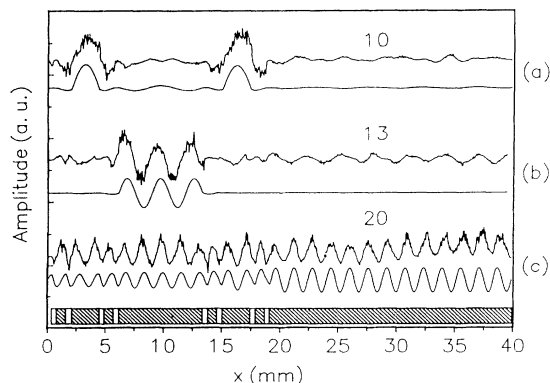


FIG. 3. Examples of normal vibration amplitude profiles of (a),(b) localized and (c) extended modes. For each mode, top (bottom) panels contain the measured (calculated) displacements. A sketch of the sample geometry is given on the abscissa (dashed, ceramic; white, resin). Only a part of the sample is represented here, due to the mirror-plane symmetry with respect to its central plane ($x = 30$ mm).

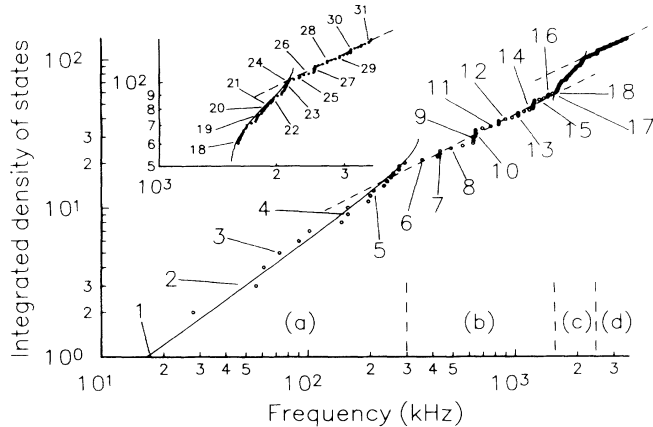


FIG. 4. Calculated log-log plot of the integrated DOS vs mode frequencies for the sample of Figs. 1 and 2; the high-frequency part is enlarged in the inset (circles). Numbers indicate the modes which have been identified in Fig. 2 on the basis of their displacements (we recall that odd-parity modes cannot be experimentally observed). Four regimes can be distinguished: In (a) and (c), the points follow the dispersion curves of the corresponding periodic sample where the smallest elements of ceramic and resin alternate (solid lines); in (b) and (d) they display a quasilinear dispersion as fitted by the dashed lines.

eigenmodes of the structure; at each of these peaks we calculated the z displacement of the wave field, u_z , knowing that this is related to the longitudinal field, u_x , by the relation $u_z \sim \partial u_x / \partial x$ [4(c),6]. The actual parameters used in the calculation are similar to those used in Ref. [4] (for the ceramic constituent, $v = 3000$ m/s, $\rho = 7.65$ g/cm³; for the epoxy constituent, $v = 1700$ m/s, $\rho = 1.17$ g/cm³). The calculated frequency spectrum is plotted on a logarithmic scale in Fig. 4, and calculated displacements corresponding to the experimental ones are shown in Fig. 3. The numbers in Figs. 2 and 4 mark those modes which have been identified in the experiment on the basis of their displacements. We believe that a comparison between theory and experiments, based on dis-

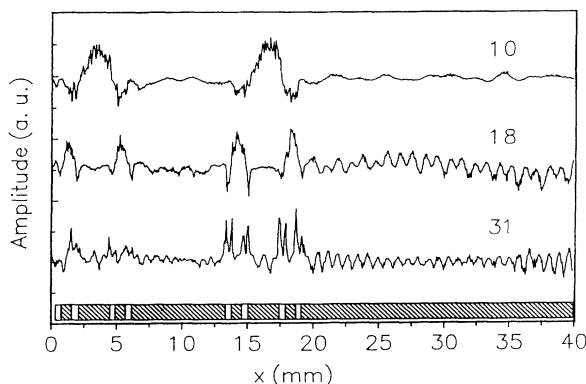


FIG. 5. Experimental normal amplitude profiles for three localized modes displaying self-similar behavior.

placements rather than merely on frequencies, is much more meaningful, as it allows us to exclude spurious experimental resonances, most of which can be unambiguously assigned to plate vibrations along lateral directions and their harmonics.

The evidence of localized fracton modes and extended phonon modes is immediately apparent from their displacements (Fig. 3). In modes 10,13 [Figs. 3(a) and 3(b)] the vibration amplitude is mostly localized on a few elements, while mode 20 [Fig. 3(c)] essentially extends to the whole sample.

A remarkable direct evidence of the self-similar nature of displacements, reflecting the self-similarity of the structure, comes from Fig. 5, where we show three localized modes of different frequencies corresponding to vibrations of "subclusters" of different scales in the same sample. To our knowledge this is the first experimental evidence of self-similarity in the displacement patterns [7].

As expected, the different localization of mode displacements closely reflects the clear crossovers in the slope of the integrated DOS (Fig. 4): A first crossover occurs between the long-wavelength region of extended modes (a) and the subsequent region of localized modes (b), which extends up to a second crossover to the so-called "particle regime" (c). However, we find that a second fracton region (d) appears at higher frequencies, also limited by a distinct crossover to region (c). This evidence is extremely clear both theoretically and experimentally, from our integrated DOS (Fig. 4) and from the displacement patterns. For example, while the first two modes of Fig. 5 belong to the fracton region (b), the third one falls in region (d) [8]. Those modes of our Cantor sample which have extended displacement profiles follow very closely the dispersion of the corresponding periodic sample [9]; indeed, both the integrated DOS and the band edges shown by the solid lines in Fig. 4 for this periodic structure seem to correspond closely to the ob-

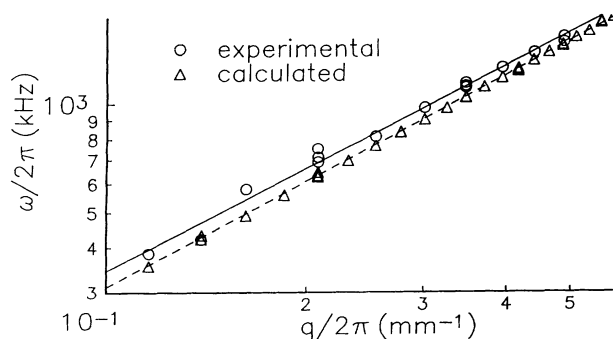


FIG. 6. Frequency vs fracton wave vector q for modes in the fracton regime (b). Circles and triangles represent experimental and theoretical data, respectively (the error in determining q is approximately 5%). Solid and dashed lines are the corresponding linear fits.

served data for the extended modes of the Cantor sample. This is true not only for region (a), but—even more clearly—for region (c) where indeed the mode displacements are also definitely extended [see, e.g., Fig. 3(c)]. As soon as their displacements are localized, the modes begin to deviate from the periodic dispersion; it is not surprising to find that indeed they fall in the successive gaps of the periodic structure. In brief, we are now interpreting the Cantor structure as obtained by inserting many "defects" in an otherwise periodic structure based on the smallest elements, which are in fact the most numerous. In this view, we are led to a generalization of the notion of fracton regime, since we do expect that localized modes will appear whenever a gap is present between the extended mode bands. Our experiments were able to detect only two of these fracton regimes [regions (b) and (d)], but further extended-mode bands and localized-mode regions may exist also at higher frequencies.

The dispersion of fracton modes in a log-log scale follows a quasilinear behavior which is fitted by dashed lines in Fig. 4. We find that the slope of the lines corresponding to regions (b) and (d) is very similar, and yields a spectral dimension $d_s \approx 0.67$, approximately equal to the fractal dimension $D = \ln(2)/\ln(3) = 0.63$. A further illustration of region (b) is given in Fig. 6 in the form of a ω vs q plot; here q is *not* an effective wave vector of the whole structure, but a *fracton wave vector* [10] obtained as the inverse of the fracton wavelength, as measured by counting the nodes in the region where the mode is localized. Circles and triangles are the result of such an operation performed on the experimental and the theoretical data, respectively. The very small difference in frequencies and in the slope of the two fitted lines can be attributed to the slightly dispersive character of the relevant Lamb wave, neglected in the calculation [4]. Again, we find that D/d_s is very close to 1 both in the experimental and in the theoretical data.

In conclusion, we have provided direct experimental evidence of the existence of *multiple fracton* and *multiple extended-mode regimes* both in the dispersion and in the displacement patterns of a finite Cantor sample. We believe that our findings may be of interest to more complex fractal structures, and hope that they will stimulate further experimental and theoretical work.

We are grateful to H. E. Roman for useful discussions and to M. Acciarini for expert technical assistance. Partial financial support by CNR, Progetto Finalizzato "Materiali Speciali per Tecnologie Avanzate" and Progetto Finalizzato "Calcolo Parallelo" (Grant No. 90.00658. PF69), is acknowledged.

^(a)Also at Dipartimento di Energetica, Università degli Studi di Roma "La Sapienza," Roma, Italy.

[1] See, e.g., A. Aharony, O. Entin-Wohlman, S. Alexander,

- and R. Orbach, *Philos. Mag.* **B 56**, 949 (1987), and references therein.
- [2] S. Alexander and R. Orbach, *J. Phys. (Paris), Lett.* **43**, L625 (1982); R. Rammal and G. Toulouse, *J. Phys. (Paris), Lett.* **44**, L13 (1983).
- [3] See, e.g., (a) J. H. Page and R. D. McCulloch, *Phys. Rev. Lett.* **57**, 1324 (1986); (b) A. Fontana, F. Rocca, and M. P. Fontana, *Phys. Rev. Lett.* **58**, 503 (1987); (c) A. J. Dianoux, J. N. Page, and H. M. Rosenberg, *Phys. Rev. Lett.* **58**, 886 (1987); (d) R. Calemczuk, A. M. De Goer, B. Salce, R. Maynard, and A. Zarembowitch, *Europhys. Lett.* **3**, 1205 (1987); (e) E. Courtens, R. Vacher, and E. Stoll, *Physica (Amsterdam)* **38D**, 41 (1989), and references therein; R. Vacher, E. Courtens, G. Coddens, A. Heidemann, Y. Tsujimi, J. Pelous, and M. Foret, *Phys. Rev. Lett.* **65**, 1008 (1990).
- [4] (a) A. Alippi, F. Craciun, and E. Molinari, *Appl. Phys. Lett.* **53**, 1806 (1988); (b) A. Alippi, F. Craciun, and E. Molinari, *J. Appl. Phys.* **66**, 2828 (1989); (c) A. Alippi, A. Bettucci, and F. Craciun, *J. Appl. Phys.* **70**, 4004 (1991).
- [5] B. B. Mandelbrot, *The Fractal Geometry of Nature* (Freeman, New York, 1983).
- [6] B. A. Auld, *Acoustic Fields and Waves in Solids* (Wiley Interscience, New York, 1973), Vol. II, p. 76.
- [7] With our choice of sample parameters (same acoustic path in ceramic and epoxy elements), self-similarity appears very clearly also in the frequency spectrum, as will be discussed elsewhere [F. Craciun, A. Bettucci, E. Molinari, A. Petri, and A. Alippi (to be published)]. This evidence is instead hindered by other choices of parameters [V. V. Konotop, O. I. Yordanov, and I. V. Yurkevich, *Europhys. Lett.* **12**, 481 (1990)].
- [8] Being very close in frequency to the edge of the extended-mode bands, the last two patterns of Fig. 5 show nonzero amplitude outside the localization region. Similarly, *resonances* with fracton character appear also *within* the extended-mode bands (Ref. [8]).
- [9] The periodic sample is made of 30 unit cells formed by the smallest ceramic and epoxy elements in the Cantor sample.
- [10] M. Montagna, O. Pilla, G. Viliani, V. Mazzacurati, G. Ruocco, and G. Signorelli, *Phys. Rev. Lett.* **65**, 1136 (1990).

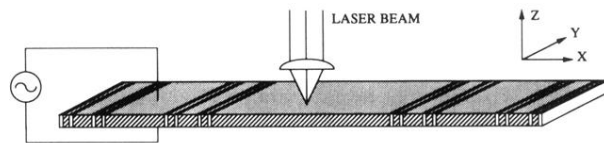


FIG. 1. Sketch of the experimental setup; an electric field applied on the electrodes excites Lamb waves which are propagating along the plate. The normal displacement component is measured by an interferometric laser probe.